Biochemical Mechanisms for Regulating Protrusion by Nematode Major Sperm Protein

Jelena Stajic[†] and Charles W. Wolgemuth[†‡*]
[†]Center for Cell Analysis and Modeling, and [‡]Department of Cell Biology, University of Connecticut Health Center, Farmington, Connecticut

ABSTRACT Crawling motion is ubiquitous in eukaryotic cells and contributes to important processes such as immune response and tumor growth. To crawl, a cell must adhere to the substrate, while protruding at the front and retracting at the rear. In most crawling cells protrusion is driven by highly regulated polymerization of the actin cytoskeleton, and much of the biochemical network for this process is known. Nematode sperm utilize a cytoskeleton composed of Major Sperm Protein (MSP), which is considered to form a simpler, yet similar, crawling motility apparatus. Key components involved in the polymerization of MSP have been identified; however, little is known about the chemical kinetics for this system. Here we develop a model for MSP polymerization that takes into account the effects of several of the experimentally identified cytosolic and membrane-bound proteins. To account for some of the data, the model requires force-dependent polymerization, as is predicted by Brownian ratchet mechanisms. Using the tethered polymerization ratchet model with our biochemical kinetic model for MSP polymerization, we find good agreement with experimental data on MSP-driven protrusion. In addition, our model predicts the force-velocity relation that is expected for in vitro protrusion assays.

INTRODUCTION

Many eukaryotic cells migrate by a process known as crawling. Cells of the slime mold *Dictyostelium discoideum* crawl to aggregate and migrate as a collective unit during colony starvation (1). Keratocytes and fibroblasts crawl during wound healing (2), and human neutrophils crawl to track down pathogens in the body (3). A single crawling cycle consists of three often-interconnected processes: extension of the leading edge, advancement of the cell body, and retraction of the rear (4–6). The first of these processes, the extension of the leading edge, is the most carefully studied (7) and found to be dependent on the polymerization of the actin cytoskeleton (5).

Polymerization of actin at the leading edge of crawling cells is a complex and highly regulated biochemical process. The fundamental biochemistry of this process is encapsulated in the dendritic nucleation model (8,9). This model describes how binding of ligand to cell surface receptors produces signals, such as the activation of Rho family GTPases, that lead to the activation of WASP family proteins (10). These proteins stimulate the Arp2/3 complex to nucleate actin polymerization (10–13), which pushes out the leading edge of the cell. Growth of an actin filament can be terminated by capping of the growing barbed end (14–16). As the actin filaments grow, they can also depolymerize due to ATP hydrolysis and severing, which replenishes the pool of G-actin in the cell (9). Mathematical models that simulate aspects of the chemical and physical processes involved in cell motility have been developed and have provided new insights into the complex processes that drive protrusion (a recent review of the field is given in (17)).

Unlike mammalian sperm, which swim to reach the egg, nematode sperm cells crawl using a physical mechanism similar to that of other crawling cells (18); however, the polymerizing protein that composes the cytoskeleton is Major Sperm Protein (MSP), rather than actin. Two major differences exist between actin and MSP: MSP forms apolar filaments and does not bind ATP (19). In addition, no molecular motors have been identified that bind to MSP. Therefore, it has been suggested that MSP-based crawling is powered solely by the biochemical and biophysical dynamics of the MSP network, making it a simpler motility apparatus than its actin-based counterparts. This simplicity makes it a good model system for studying leading edge protrusion and crawling motility in general: whereas actin is involved in numerous processes in the cell and thus regulated in a complicated manner by a host of proteins, the sperm cell is specialized for movement, and its chemical regulation is arguably much simpler.

Biochemical experiments have identified a number of key proteins involved in the regulation of MSP polymerization in nematode sperm (20–22). Many of these experiments are carried out using an in vitro system consisting of inside-out membrane vesicles and the cytosol extract (23). When ATP is added to this mixture, MSP polymerizes at the surface of the vesicles forming helical subfilaments, which pair up into (also helical) filaments, and further interlink into meshworks called fibers. The resulting structure is similar to actin comet tails formed during in vitro polymerization assays on the surface of the bacterium *Listeria monocytogenes* and coated lipid vesicles (24). The rate of fiber elongation is measured and found to be correlated with the

Submitted March 27, 2009, and accepted for publication May 19, 2009.

*Correspondence: cwolgemuth@uchc.edu

Editor: Denis Wirtz.

0006-3495/09/08/0748/10 $2.00

doi: 10.1016/j.bpj.2009.05.038

concentration of several cytosolic, and one membrane-bound, proteins (20–22). These proteins have been assigned putative roles (20,22,25) based on their influence on the elongation rate (e.g., capping protein, polymerization organizing protein, etc.). It is known that this list of regulating proteins is incomplete, since attempts to recreate fiber growth in a mix of artificially synthesized proteins have proven unsuccessful. Nevertheless, as quantitative data is available, it is important to elucidate the mechanisms of regulation that the hitherto discovered proteins employ. Indeed, as nematode sperm motility has been used as a model system for constructing mathematical models to describe the biophysics of crawling (26–30), a quantitative model describing the biochemical kinetics in this system will provide a means for connecting the biophysical crawling mechanisms to the internal chemical regulation.

In this article, we develop a mathematical model for the biochemical kinetics of MSP protrusion, based on the biological model developed through experimentation. We make the assumption that the rate of MSP fiber elongation is equal to the filament polymerization rate. The roles assigned to different regulating proteins are found to be consistent with available data. We also find that it is not satisfactory to treat the polymerization as if it were happening in free space: The proximity of the membrane (or the vesicle) needs to be accounted for by using a model that incorporates feedback between the number of actively polymerizing filaments and the polymerization rate. Therefore, we chose to use the tethered-ratchet model developed by Mogilner and Oster (31) to accurately capture the elongation rate's dependence on a putative capping protein. Our model is able to fit existing experimental data, thereby providing estimates for the kinetic parameters for this system. In addition, the model provides predictions for the force-velocity relation for MSP-driven protrusion.

Experimental background

Using a number of biochemical techniques, such as fractionation and reconstitution, some of the proteins required for fiber formation and elongation have been discovered (20–22). Dilution experiments were performed using the in vitro system introduced in Italiano et al. (23) to measure the dependence of fiber elongation rate on the concentrations of these proteins. These experiments yielded several key observations:

1. The MSP concentration in the system does not influence the elongation rate (23). This result is of course specific to the experimental conditions and is not expected to remain true down to very small MSP concentrations.
2. Only one membrane-bound protein is required for fiber growth. This protein, termed MSP Polymerization Organizing Protein, or MPOP, is active in its phosphorylated form and designates the sites of MSP polymerization and fiber formation on the surface of the vesicle (or the leading edge of the sperm cell) (20).
3. Two cytosolic proteins, called MSP fiber proteins (MFP1 and MFP2), affect the rate of fiber elongation (21). MFP2 is required for fiber formation and has been demonstrated to increase the rate of fiber elongation; MFP1, on the other hand, suppresses this rate. Both proteins are incorporated into MSP fibers, with the degree of MFP2 phosphorylation decreasing steadily along the fiber as one moves away from the vesicle.
4. A cytosolic kinase, termed MSP polymerization-activating kinase (MPAK), is also required for fiber growth (22). MPAK is recruited to the membrane by MPOP, where it phosphorylates MFP2.

A more detailed view of the influence of MFP1 and MFP2 on the fiber elongation rate is presented in Fig. 1, which contains data from Fig. 4 of Buttery et al. (21) (see our Fig. 1, *A* and *B*) and Fig. 2 *d* of Italiano et al. (23) (see our Fig. 1 *C*). Our figure depicts the mean rates of fiber

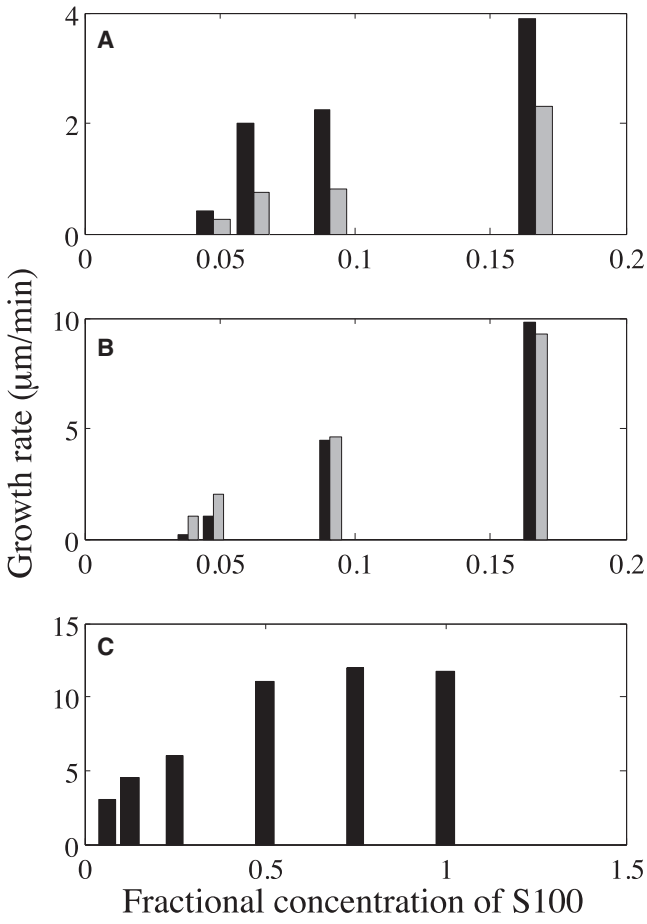

FIGURE 1 (*A* and *B*) Redrawn from Figs. 4, *A* and *B*, respectively, in Buttery et al. (21). (*C*) Redrawn from Fig. 2 *d* in Italiano et al. (23). *X* axis: Fractional concentration of S100 (e.g., the value of 0.5 corresponds to the 1:1 dilution of S100 with KPM buffer). (*Solid bars*) Fiber elongation rates for varying dilutions of S100. (*Shaded bars*) Corresponding elongation rates with MFP1 (*A*) or MFP2 (*B*) added at the same concentration at all dilutions. This concentration is equal to $\overline{F_1}$ for MFP1 and 0.88 $\overline{F_2}$ for MFP2, where $\overline{F_1}$ and $\overline{F_2}$ are the respective concentrations of MFP1 and MFP2 in S100.

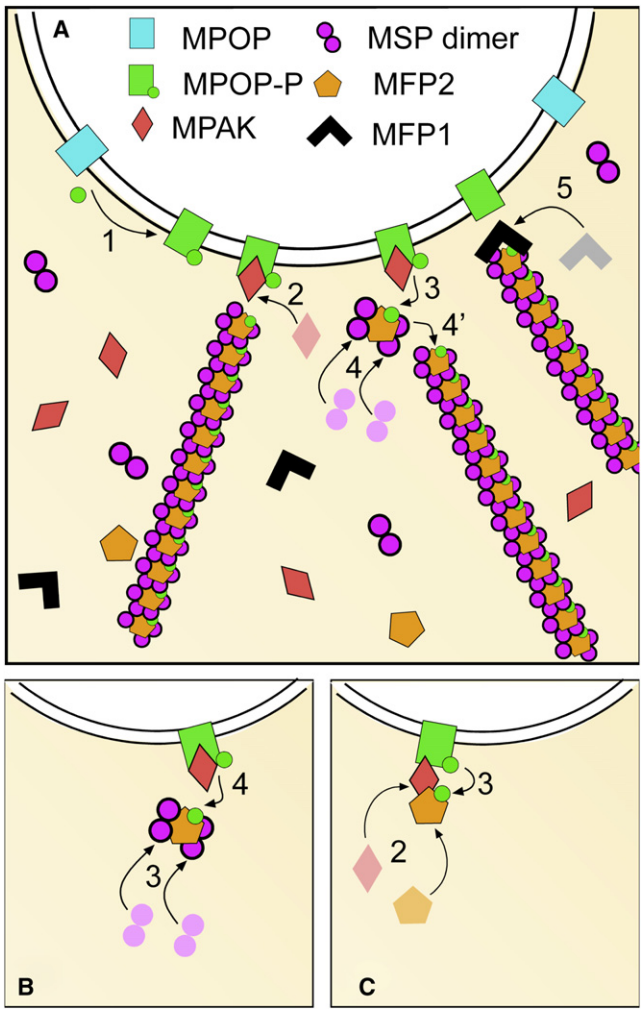

FIGURE 2 Schematic representation of the biochemical model of MSP polymerization in artificial assays. Shaded area represents the solution, whereas the open area is the membrane vesicle. (*A*) Step 1: Phosphorylation of MPOP by an unknown mechanism. Step 2: Recruitment of MPAK (*red*) by the phosphorylated MPOP (*green*). Step 3: Phosphorylation of MFP2 (*orange*) by MPOP-bound MPAK. Step 4: Binding of MFP2 and MSP dimers (*purple*) and elongation of an existing filament. Step 5: Capping of a polymerizing filament by MFP1 (*black*). (*B*) Alternative binding scenario. (Following Steps 1 and 2 from panel *A*). Step 3: Binding of MFP2 to MSP dimers. Step 4: Phosphorylation of MFP2 by MPAK. (*C*) Alternative binding scenario. (Following step 1 from panel *A*). Step 2: Binding of MFP2 and MPAK in solution. Step 3: Recruitment of the MFP2-MPAK complex to the membrane and phosphorylation of MFP2 by MPOP-bound MPAK.

elongation in systems in which the sperm cell supernatant (S100) was diluted with KPM buffer (0.5 mM $MgCl_2$, 10 mM potassium phosphate, pH 6.8); the solid bars are the elongation rates in the diluted cell extract, whereas the shaded bars are the rates for the same dilution ratio, but with MFP1 (Fig. 1 *A*) or MFP2 (Fig. 1 *B*) added at their natural concentration in the cytosol. It is clear that MFP1 has a suppressing, and MFP2 an enhancing, effect on the growth rate; in the case of MFP2, the more diluted the extract, the more this effect increases. Fig. 1 *C* shows growth rates for a different range of KPM:S100 dilution ratios.

Structural studies of MSP and MFP2 proteins were also conducted (19,25,32). MSP forms dimers, which polymerize into helices: this structure is called a subfilament. The angle between successive MSP dimers in a subfilament was found to be ~100°. On the other hand, MFP2 consists of two domains connected by a linker; the domains are rotated with respect to each other by an angle of ~110° (25). The dimensions of an MSP monomer and a single MFP2 domain are comparable: 15 Å × 20 Å × 45 Å for MSP (19), vs. 24 Å × 36 Å × 42 Å for MFP2 (25).

The model

From the experimental findings described in the previous section, the following biochemical model is suggested: Following its phosphorylation by an unknown mechanism, MPOP (a membrane protein) recruits MPAK to the membrane. There, MPAK phosphorylates MFP2, thus activating it. Since MFP2 gets incorporated into fibers and is required for fiber formation, we assume that MSP dimers bind to activated MFP2 for polymerization. Indeed, it has even been suggested that MFP2 might act as a staple between two MSP dimers, since the angle between two consecutive MSP dimers in a subfilament is roughly equal to the angle between the two domains in an MFP2 molecule (25); however, we will not assume any specific molecular level structure for the binding of MFP2 and MSP dimers. We can also assume that MFP2 gets dephosphorylated after already being incorporated into a fiber when it no longer needs to be active, which accounts for its decreased phosphorylation along the fiber. The growth of the subfilament is finally terminated by MFP1, which acts as a capping protein, and also remains incorporated in the fiber.

In this article, we are interested in modeling the previously-mentioned in vitro protrusion assays. These experiments are carried out in a roughly 20 μL volume of fractionated supernatant, which is many orders-of-magnitude larger than the volume of a polymerizing fiber complex, which are typically microns in diameter and tens of microns long (21,23). Therefore, we assume that the amount of MSP incorporated into fibers does not significantly change the bulk concentration of free, unpolymerized MSP. This assumption is also applied to the other cytosolic proteins in the model, such as MFP1, MFP2, and MPAK; thus, we consider the concentration of all the cytosolic proteins in the supernatant fraction to be constant during fiber formation. Another assumption is that we consider the fiber elongation rate to be equal to the polymerization rate, decreased by any depolymerization that might be taking place at the membrane.

The mechanisms listed in the biochemical model do not fully constrain the mathematical model we are about to build. For example, MPAK could first be recruited to the membrane, then recruit MFP2 and phosphorylate it; the

phosphorylated MFP2 would then bind MSP dimers and form a new polymerization link on an existing filament (see Fig. 2 *A*). Alternatively, MFP2 and two MSP dimers could first form a preformed link for the polymerizing chain, which would then be recruited to the membrane by MPAK and primed for polymerization by the phosphorylation of MFP2 (Fig. 2 *B*). Finally, MPAK and MFP2 could bind in the cytosol, then be recruited to the membrane by phosphorylated MPOP, where MFP2 would be phosphorylated making it capable of binding MSP dimers (Fig. 2 *C*). We will attempt to distinguish between these alternatives using the elongation data available.

Let us begin by examining the reaction scheme depicted in Fig. 2 *A*. In the reactions to follow, phosphorylated chemical species are marked with an asterisk, and complexes are denoted with a dot between the constituents. We will assume that the binding of MPAK to phosphorylated MPOP is a reversible, second-order reaction with on-rate k_1 and off-rate k_{-1}:

$$\mathrm{MPOP}^* + \mathrm{MPAK} \underset{k_{-1}}{\overset{k_1}{\rightleftharpoons}} \mathrm{MPOP}^* \cdot \mathrm{MPAK}. \tag{1}$$

We model the binding of MFP2 and its subsequent phosphorylation as an enzymatic process obeying Michaelis-Menten kinetics with equilibrium constant $K_\mathrm{m} = k_{-2}/k_2$, where k_2 and k_{-2} are forward and reverse reaction rates for the intermediate complex formation. Activated (phosphorylated) MFP2 is then released from the membrane with rate k_3,

$$\begin{aligned}\mathrm{MFP2} + \mathrm{MPOP}^* \cdot \mathrm{MPAK} + \mathrm{P} \underset{k_{-2}}{\overset{k_2}{\rightleftharpoons}} \mathrm{MFP2}^* \cdot \mathrm{MPOP}^* \cdot \mathrm{MPAK} \\ \overset{k_3}{\rightarrow} \mathrm{MFP2}^* + \mathrm{MPOP}^* \cdot \mathrm{MPAK}\end{aligned}, \tag{2}$$

where P is the phosphate group. Finally, MFP2* binds to two MSP molecules and the end of an existing MSP filament, which adds a new link to that polymer chain at a rate k_4:

$$\mathrm{MFP2}^* + 2\mathrm{MSP} + \mathrm{Filament} \overset{k_4}{\rightarrow} \mathrm{Link} + \mathrm{Filament}. \tag{3}$$

We now describe the preceding system of chemical reactions in mathematical terms. For ease of reference, we include a list of all the symbols used to denote chemical concentrations in Table 1. The reaction in Eq. 1 leads to the following equilibrium value of MPAK-bound phosphorylated MPOP,

$$AO = \frac{O_\mathrm{t}\ A}{A + K_1}, \tag{4}$$

where $K_1 = k_{-1}/k_1$ and $O_\mathrm{t} = O + AO$. We also assume that the creation rate of the phosphorylated MFP2 is balanced by the rate of its depletion due to the polymerization reaction:

$$k_3 \frac{AO\ F_2}{F_2 + K_\mathrm{m}} = \frac{dL}{dt} = C_1\ O_\mathrm{t}\ V_P. \tag{5}$$

TABLE 1 Names of species concentrations

Symbol	Definition
O	Surface concentration of phosphorylated MPOP available for binding.
A	Concentration of MPAK.
AO	Surface concentration of phosphorylated MPOP bound to MPAK.
O_t	Total surface concentration of phosphorylated MPOP equal to $O + AO$.
F_1	Concentration of MFP1.
F_2	Concentration of MFP2.
F_2*	Concentration of phosphorylated MFP2.
AOF_2	Surface concentration of the complex consisting of phosphorylated MFP2, phosphorylated MPOP, and MPAK.
S	Concentration of MSP dimers.
L	Concentration of links in the polymerization chains of MSP filaments.

The second equality comes from the fact that V_p is the polymerization rate averaged over the section of the vesicle surface populated by the phosphorylated MPOP, with C_1 as the proportionality constant. Equations 4 and 5 lead to the following dependence of the elongation rate V on the concentrations of MFP2 and MPAK,

$$V = C\frac{A}{A + K_1}\frac{F_2}{F_2 + K_\mathrm{m}} - V_\mathrm{dep}, \tag{6}$$

where $C = k_3/C_1$, and V_dep is the average depolymerization velocity at the vesicle.

Similarly, for the binding scenarios described in Fig. 2, *B* and *C*, we obtain

$$V = C\frac{A}{A + K_1}\frac{F_2\ S^2}{F_2\ S^2 + K_\mathrm{m}} - V_\mathrm{dep} \tag{7}$$

for the preformed MFP2 -2 MSP binding (Fig. 2 *B*), and

$$V = C\frac{A\ F_2}{A\ F_2 + K_\mathrm{m}} - V_\mathrm{dep} \tag{8}$$

for the preformed MPAK-MFP2 binding (Fig. 2 *C*). Constants C, K_1, and K_m have interpretations similar to those in Eq. 6.

Notable in Eqs. 6–8 is the absence of dependence on the capping protein, MFP1. This is because we assume that the average polymerization rate does not depend on the number of actively-polymerizing filaments. Since the total number of growing filaments must produce enough force to push the vesicle at the observed velocity, the average force that each filament feels depends on the total number of growing filaments. Capping of filaments by MFP1 can lead to a reduced number of growing filaments and, therefore, would increase the force experienced by each filament, which is expected to decrease the average polymerization rate. Consistent with this idea, MFP1 concentration has a considerable influence on the fiber elongation rate (Fig. 1 *A*), which is not accounted for in the chemical reaction model developed above.

To address this, we describe the MSP polymerization-driven protrusion more accurately using the tethered-polymerization ratchet model (31). This model has its origins in the so-called Brownian-ratchet mechanism, which was first introduced by Peskin et al. (33) to explain actin-polymerization-driven cell motility, and in which a stiff actin filament is pushing a thermally fluctuating membrane. This model was later improved upon by Mogilner and Oster (31,34); in these works, the spatial gap between the tip of the actin filament and the membrane, which is necessary for further polymerization, is created by the bending of the actin filament (i.e., the elastic Brownian ratchet). In addition, the experimental observation that actin filaments remain attached to the membrane for some time after being nucleated has also been taken into account (31). These models are appropriate for the nematode sperm system since the in vitro MSP filaments have been found to have mechanical properties similar to actin (35): They are semiflexible, with a persistence length of ~9 μm (compared to 7–10 μm for actin) and an average filament length of 0.67 μm. Because external forces applied to the vesicle or the filament can inhibit the thermal fluctuations that open the gaps enabling polymerization, these Brownian ratchet-type models predict a reduction in the polymerization velocity due to resistive forces.

In the tethered-ratchet model (31), the experimentally observed molecular link between a recently nucleated actin filament and the membrane is modeled as a spring, which is connected in-series to the more elastic actin filament (the effective strength of the molecular link is labeled f_b, whereas the spring coefficient of the actin filament is called k). The attachment through the molecular link breaks with a free dissociation rate of δ_0. After the breakage, the formerly attached filament becomes a working filament, since it is able to bend, creating enough space to polymerize, and providing a propulsion force for the membrane. Eventually, the filament is capped and loses contact with the membrane. Because the gap between the end of a working filament and the vesicle is not always large enough to allow for the intercalation of an MSP dimer, the velocity of polymerization is lower compared to its value in free space V_{max} (31),

$$V = V_{max} e^{-f_w/k_B T} - V_{dep}, \tag{9}$$

where f_w is the force exerted by a single working filament, k_B is the Boltzmann constant, and T is temperature. In our system, we can assume that the viscous forces experienced by the vesicle are negligible in comparison with the forces generated by the cytoskeleton. Thus the pushing forces created by the working filaments are balanced out by the pulling forces of attached filaments, leading to the following force-balance equation (per-filament pulling force denoted by f_a),

$$f_a\ a = f_w\ w, \tag{10}$$

where a and w are, respectively, the number of attached and the number of working filaments. We further assume that an equilibrium has been reached among the attached, working, and capped filaments, so that

$$a/w = k/\delta, \tag{11}$$

where κ is the capping rate and δ is the rate of the molecular link breakage under tension force f, $\delta \approx \delta_0 \exp[-f/f_b]$ (31). Following the derivation in Mogilner and Oster (31), we compute the velocity of polymerization as

$$V = V_{max} \exp\left[-l\left(f_b \nu \omega^2(\nu)(\kappa/\delta_0)\right)/k_B T\right] - V_{dep}, \tag{12}$$

where V_{max} is the free polymerization velocity, i.e., the first term in Eq. 6 and its equivalents, Eqs. 7 and 8. In addition, l is the increase in length of the polymer due to the addition of a single MSP dimer, and ν is the dimensionless velocity V/V_0 with the velocity scale $V_0 \equiv f_b\delta_0/k$, whereas

$$\omega(\nu) \equiv \int_0^\infty dx\, x \exp\left[\nu x + \frac{1 - e^{\nu x}}{\nu}\right]. \tag{13}$$

Thus, we have recovered the dependence of the elongation rate on the capping rate (in turn dependent on the concentration of MFP1).

Combining Eqs. 6 and 12, we find the following functional form for the growth rate,

$$\begin{aligned} \nu &= \alpha \frac{A}{A + K_1} \frac{F_2}{F_2 + K_m} e^{-\frac{F_1}{\beta}\nu\omega^2(\nu)} - \nu_{dep} \\ \nu &\equiv V/V_0 \\ \nu_{dep} &\equiv V_{dep}/V_0, \end{aligned} \tag{14}$$

with fitting parameters $\alpha \equiv C/V_0$, $\beta \equiv (\delta_0/\overline{\kappa})\ (k_B T/(l f_b))\overline{F_1}$, K_1, K_m, ν_{dep}, and V_0, where $\overline{\kappa}$ and $\overline{F_1}$ are the values of the capping rate and MFP1 concentration in undiluted S100, respectively. Similar expressions can be obtained by extracting V_{max} from Eqs. 7 or 8 instead of Eq. 6. When comparing with the experimental results, the concentrations of cytosolic proteins MFP1, MFP2, and MPAK will be corrected by a dilution factor x (e.g., $F_1 = x\overline{F_1}$, where $x = 1/(n + 1)$ for a 1:n dilution of S100). We will now attempt to fit the available data to the above functional form.

RESULTS

Proceeding to test the model, we note first a discrepancy in the KPM data between panels *A* and *B* of Fig. 1: The growth rates at the same dilution ratios are roughly twice as high in Fig. 1 *B* than in panel *A* due to the fact that the experiments were done using different batches of sperm extract (T. Roberts, Florida State University, personal communication, 2008). To increase the number of fitting points, we decided to also use the data in panel *C*; these data points cover a range of dilutions that is complementary to that in panels *A* and *B*, with the growth rate values that seem consistent with the numbers from panel *A*. Thus, we will fit the combined data from panels *A* and *C* of Fig. 1; the data

from panel *B* will be fitted with a separate set of parameters. To find the values of fit parameters, we minimize the function χ^2,

$$\chi^2 = \sum_{i=1}^{i=N} \left(V_i^{exp} - V_i^{th}\right)^2 / \sigma_i^2, \quad (15)$$

where N is the number of experimental points, whereas V_i^{exp}, V_i^{th}, and σ_i are, respectively, the values of the measured velocity, modeled velocity, and experimental error, all at the i^{th} experimental point. The minimization is performed over six parameters (α, K_1, K_m, β, ν_{dep}, and V_0) with associated experimental errors σ_i extracted from the literature (21,23). We use the global minimization routine NMinimize under Mathematica 6.0 (Wolfram Research, Champaign, IL), choosing the option NelderMead (simplex optimization) for the method.

We first attempt to distinguish between the different binding scenarios represented in Fig. 2, *A–C*, and Eqs. 6–8. As each of these expressions has a distinct form of the growth-rate dependence on MFP2 concentration, we will use the data of Fig. 1 *B* to fit Eq. 14 and its equivalents. From Fig. 1 *B* it is clear that the growth rate for both sets of data (simple KPM dilution and MFP2 added at a constant concentration) has a roughly linear dependence on the fractional concentration of S100 (which we call x). Therefore, it is not surprising that the MPAK-MFP2 binding scenario (Eq. 8 and Fig. 2 *C*) does not yield a satisfactory fit (results not shown): for small x, such as in the experiment, the maximum elongation rate will be linear in x when F_2 is held constant, but will have a quadratic dependence on x for the simple KPM dilution. However, when V_{max} is extracted from either of the other two scenarios (Eq. 6 or Eq. 7; Fig. 2, *A* or *B*), we obtain very good agreement with the experimental data (see Fig. 3), yielding a small value for the Michaelis-Menten constant K_m. This is to be expected since a small K_m attenuates the dependence on F_2 which, as in the experiment, only becomes significant at very low x. Thus, with the limited available data we are unable to distinguish between the scenario in which MFP2 and two MSP dimers form a link first and then make contact with MPAK at the membrane and polymerize, and that in which MFP2 is recruited to the membrane first, is activated, and then binds the MSP dimers in order to allow polymerization. In the remainder of this work, we will use the latter scenario (Eqs. 6 and 14; Fig. 2 *A*) to fit the experimental data.

We will now use the rest of the data to further constrain the fitting parameters. As mentioned above, it is not possible to fit all of the data in Fig. 1 with a single set of parameters. However, we note that the KPM data in panels *A* and *B* of that figure seem to differ from each other by a multiplicative factor; thus we can try to fit the combined data with a single parameter set, save for the overall velocity scale V_0. We obtain a very good fit to all the data from Fig. 1, with the results shown in Fig. 4. Fig. 4 *A* shows the fits to the

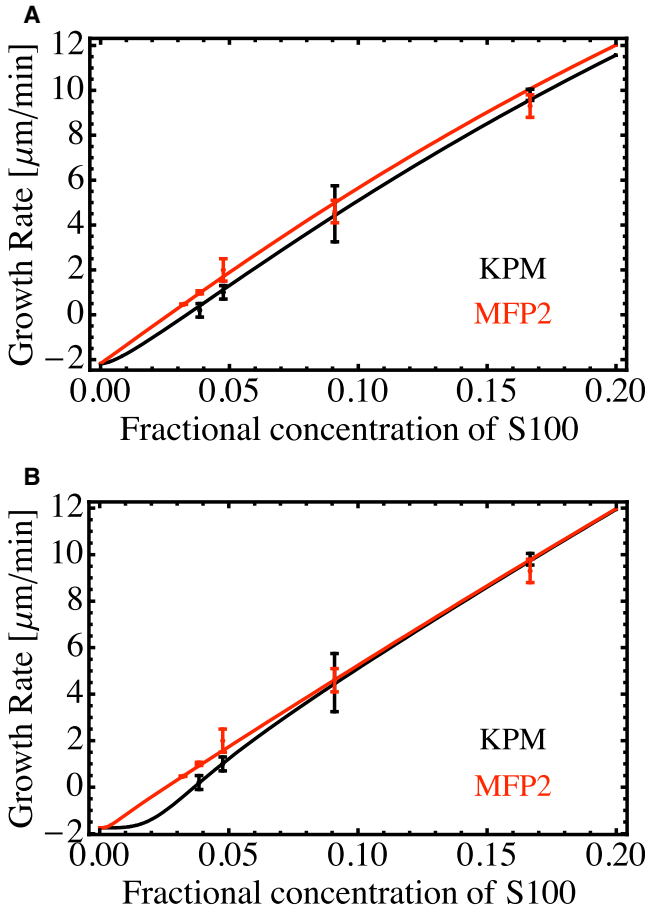

FIGURE 3 Fits to elongation rate data from Fig. 1 *B*. (*A*) Results for the binding scenario depicted in Fig. 2 *A*. (*B*) Results for the binding scenario depicted in Fig. 2 *B*. The data obtained by a simple dilution of the cell extract with the KPM buffer is shown in black, whereas the data with the MFP2 concentration held constant is shown in red. In both panels, the fit functions are represented by lines and the experimental data by symbols with error bars.

combined data from Fig. 1, *A* and *C*, and Fig. 4 *B* the fits to the data from Fig. 1 *B* with the value of the parameter V_0 roughly twice as large. The complete set of parameter values that yielded the plots in Fig. 4 is given in Table 2, with V_0^{MFP1} and V_0^{MFP2} being the values of the parameter V_0 used in Fig. 4, *A* and *B*, respectively.

In any study involving model fitting with multiple parameters, it is possible to have numerous local minima in χ^2 that are all very close in magnitude to the global minimum. If a parameter has a consistent value for all these minima, then we define that parameter as being robust. To assess the robustness of our fit parameters, we performed a minimization of the χ^2 function by finding local minima in the vicinity of ~1000 starting points from our parameter space. We found that multiple local minima have a χ^2 very close to the value corresponding to the fitting parameters in Table 2. Table 3 summarizes our conclusions about the robustness of the fit parameters. Although the parameters α and K_1 are not independently robust, the combination

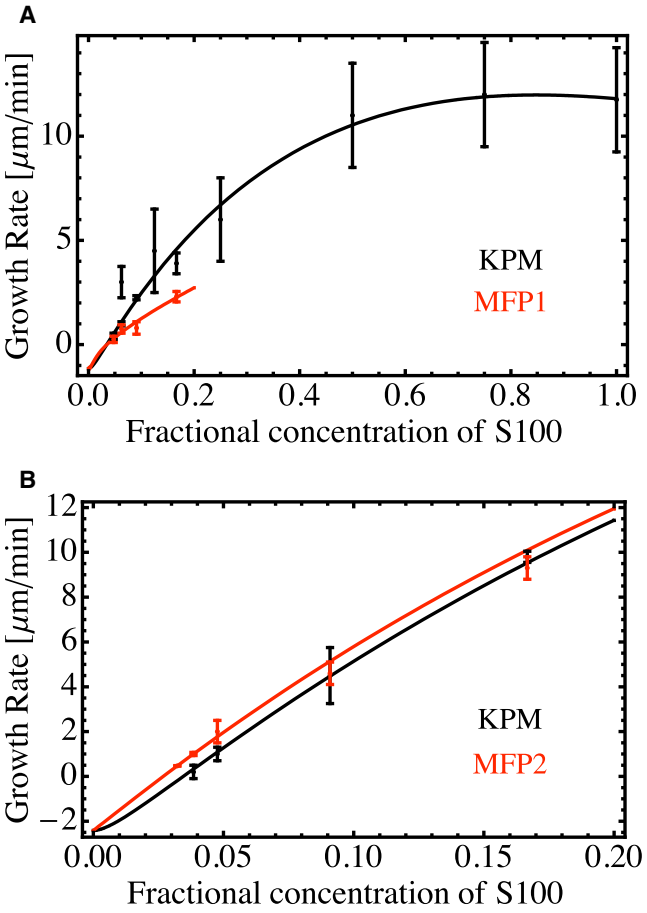

FIGURE 4 (*A*) Fits to combined elongation rate data from panels *A* and *C* of Fig. 1. (*B*) Fits to elongation rate data from panel *B* of Fig. 1. The fitting parameters are the same for both panels, except for the parameter V_0, the overall velocity scale, which is roughly twice as large for the fits in panel *B* (see Table 2). The data obtained by a simple dilution of the cell extract with the KPM buffer is shown in black, whereas the data with MFP1 (*A*) or MFP2 (*B*) concentrations held constant is shown in red. In both panels, the fit functions are represented by lines and the experimental data by symbols with error bars.

$\alpha {V_0}^{\mathrm{MFP1}}/K_1$ is. We also find that the equilibrium constant for the binding of MPAK to phosphorylated MPOP (K_1) is always (and often considerably) greater than the concentration of MPAK in undiluted S100, indicating weak binding. As already pointed out, the subtlety of the effect of MFP2 concentration on the growth rate suggests a small Michaelis-Menten constant for the phosphorylation of MFP2, and indeed the robust fitted value for K_m in Table 3 is small in comparison to 400 μM, the concentration of MFP2 in undiluted S100. With these two results in mind, at a given dilution x we can approximate the first of the Eqs. 14 with

$$\nu = \frac{\alpha}{K_1}\overline{A}x e^{-\nu\omega^2(\nu)\frac{\overline{F_1}}{\beta}x} - \nu_{\mathrm{dep}}. \tag{16}$$

We notice that the polymerization velocity has two competing multiplicative terms, one increasing in x, and the other exponentially decreasing in x. If we were to solve the expressions in Eq. 14 for a given set of parameters (e.g., the set in Table 2) for the case of simple dilution with KPM buffer, and with values of x extending beyond 1, we would get a curve with a maximum positioned close to $x = 1$ (Fig. 5). Thus, we may estimate the parameter β from Eq. 16 by differentiating it with respect to x and setting the derivative to zero at $x = 1$. This yields the relationship

$$\beta = \overline{F_1}\overline{\nu}\omega^2(\overline{\nu}), \tag{17}$$

where $\overline{\nu}$ is the reduced velocity in undiluted S100. This is confirmed through our simulations: In the sets of parameters with minimal χ^2, the values of β and ${V_0}^{\mathrm{MFP1}}$ are correlated approximately through Eq. 17. Finally, from Eqs. 16 and 17 we have

$$\frac{\alpha}{K_1}{V_0}^{\mathrm{MFP1}} = \left(\overline{V}^{\mathrm{MFP1}} + V_{\mathrm{dep}}^{\mathrm{MFP1}}\right)\frac{e}{\overline{A}}, \tag{18}$$

where $\overline{V}^{\mathrm{MFP1}}$ is the polymerization velocity in undiluted S100 (~12 μm/min), and $V_{\mathrm{dep}}^{\mathrm{MFP1}} = {V_0}^{\mathrm{MFP1}}\nu\mathrm{dep}$ is the depolymerization velocity. Since $V_{\mathrm{dep}}^{\mathrm{MFP1}}$ is robust (Table 3), it is clear from Eq. 18 that the combination of parameters $\alpha {V_0}^{\mathrm{MFP1}}/K_1$ is also robust.

TABLE 2 Model parameters used to generate the fits in Fig. 4

Variable	α	K_1	K_m	β	ν_{dep}	${V_0}^{\mathrm{MFP1}}$	${V_0}^{\mathrm{MFP2}}$
Value	50	59 μM	4 μM	64 μM	0.34	$3.4\frac{\mu m}{\mathrm{min}}$	$7.08\frac{\mu m}{\mathrm{min}}$

To extract the values of these parameters, the following concentrations of MPAK, MFP1, and MFP2 in *S*100 were used: 15 μM, 140 μM, and 400 μM, respectively. These concentrations were obtained from the literature (21,22).

TABLE 3 Robustness of fit parameters for the model in Eq. 14

Variable	Robustness
α, K_1	Expression $\alpha {V_0}^{\mathrm{MFP1}}/K_1$ robust at $2.9\frac{\mu m}{\mathrm{min}\ \mu M}$, $K_1 \geq 30$ μM
K_m	Robust at 4 μM
${V_0}^{\mathrm{MFP1}}$	Ranges between 2.5 and $5\frac{\mu m}{\mathrm{min}}$
β	Ranges between 40 and 80 μM, depending on ${V_0}^{\mathrm{MFP1}}$
ν_{dep}	$\approx 1.2\frac{\mu m}{\mathrm{min}}/{V_0}^{\mathrm{MFP1}}$
${V_0}^{\mathrm{MFP2}}$	$\approx 2{V_0}^{\mathrm{MFP1}}$

DISCUSSION

We have constructed a mathematical model of the chemical regulation of MSP polymerization, a mechanism involved in the locomotion of nematode sperm (such as *Ascaris suum* and *Caenorhabditis elegans*). Experiments have identified some of the key proteins involved in this process; however, the function of these proteins remains fairly speculative. Therefore, we developed a model based on the putative functions of these proteins, to determine whether these are consistent with the experimental data available on the dependence of MSP fiber elongation on supernatant dilution. The model treats MFP2 and MPOP as factors that influence the

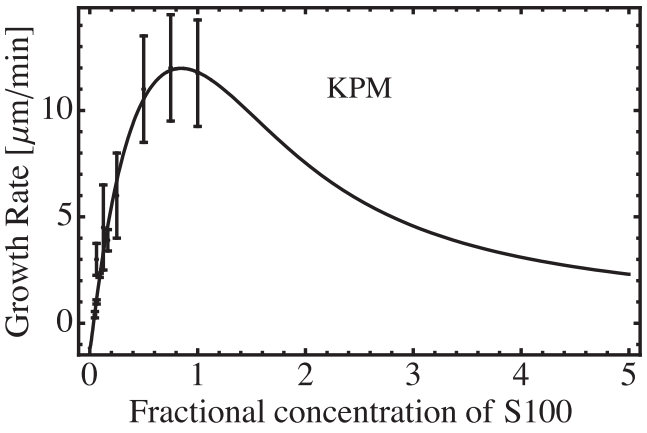

FIGURE 5 KPM data fit function from Fig. 4 *A* shown for a wider range of dilutions x (where $x > 1$ means a system that is concentrated rather than diluted with respect to the natural S100).

polymerization of MSP filaments through an enzymatic process, and treats MFP1 as a capping protein. We found that to explain the dependence of the growth rate on MFP1 concentration, we had to take into account the effect of applied force on the polymerization rate, which was modeled using the tethered polymerization ratchet model. Combining this biochemical reaction scheme and the tethered-ratchet model produced good agreement with in vitro dilution experiments. Although this model may not be the only mechanism that agrees with the experimental data, we believe that the approximations used in building the basic model are reasonable and well justified. In terms of biochemistry, we were able to show that the suggested activities of MFP1 as a putative capping protein and MFP2 as a polymerizing factor are sufficient to explain the experimental observations. On a more mechanistic level, we ruled out a possible binding-sequence scenario involving phosphorylated MPOP, MFP2, MPAK, and MSP dimers, and identified two alternatives that are compatible with the available measurements of the growth rate.

Some of our fit parameters have been measured or estimated for the actin system (e.g., V_0 is estimated at 0.3 μm/min, and V_{dep} at 0.13 μm/min (31)). Comparing these values with our results in Table 3, we find that the MSP values are larger than those for actin, but still physically reasonable. In particular, the velocity scale V_0 equal to $f_b\delta_0/k$ is roughly 10 times larger for the MSP system. This may be a consequence of a smaller spring constant k for MSP filaments, indicating that they are more stretchable than actin filaments, which are constrained by branching. The parameter $\beta/\overline{F_1}$, which is dependent on the capping rate and several mechanical properties of the filaments, ranges between 0.3 and 0.6 in our fitting, compared to 0.2 for actin (31). We also have a robust prediction (4 μM) for the Michaelis-Menten constant K_m for MFP2 phosphorylation. A direct biochemical measurement of K_m would be a good test of the validity of our model. Conversely, as the equilibrium constant for MPOP-MPAK binding K_1 does not have a robust value in our fits, its measurement would help constrain our model parameters.

As pointed out earlier, the experimental measurements from panels *A* and *B* of Fig. 1 done on two different batches of the cell extract could not be fitted with the same set of parameters. However, we showed that it is possible to only vary one parameter (the overall velocity scale V_0) between the two data sets and fit all the available data. (Note that different V_0 values also result in different depolymerization velocities.) Since the scale V_0 and the depolymerization velocity V_{dep} depend on the physical properties of MSP filaments, we speculate that the twofold difference between the values of these parameters for the two panels in Fig. 1 is due to the looser filaments formed from the batch corresponding to panel *B*.

We are also able to propose experimental measurements that might be able to test our model. One distinct feature of the model in Eq. 14 and its approximate form in Eq. 16 is the competition between $V_{\max}$, the maximum velocity in free space, and the exponential factor reflecting the space constraint. As the system becomes less diluted (x increases), the exponential takes over, and the velocity starts dropping from its maximum near $x = 1$ (Fig. 5). This behavior suggests an intriguing possibility that the system selected the physiological dilution to optimize velocity. Thus, one might test the model by measuring the velocities at $x > 1$ in search of this striking feature. However, due to experimental limitations, these conditions (concentrated, rather than diluted cell extract) might be difficult to achieve, making this test of questionable use.

Another measurement should be more experimentally tractable: If a known external force is applied on the vesicle, the force-velocity relation may be extracted. At $x = 1$ (undiluted cell extract), we can use the following expressions to calculate this relation (31),

$$\begin{aligned} v &= \alpha \frac{A}{A + K_1} \frac{F_2}{F_2 + K_m} e^{-\frac{F_L}{\beta} r\omega^2(v) - \gamma F_L} - v_{\text{dep}} \\ v &\equiv V/V_0 \\ v_{\text{dep}} &\equiv V_{\text{dep}}/V_0 \end{aligned}, \qquad (19)$$

where F_L is the load force, and $\gamma \equiv (l/k_BT)(\overline{\kappa}/n)$ with n being the nucleation rate. Fig. 6 shows our predicted force-velocity relationship. Since the nucleation rate n does not feature in our fitting formula Eq. 14, we do not have a fitted value for it. Instead, we use the value for the $\overline{\kappa}/n$ ratio estimated for actin in Mogilner and Oster (31), and equal to 0.05. Since the relevant value for MSP might be different, we also show the result for twice (*long dashes*) and half (*short dashes*) the value of that ratio. As our fitted parameters are not entirely robust, we also show the results for several optimal parameter sets (at the actin value for $\overline{\kappa}/n$), all within the ranges shown in Table 3 (*full lines*). Clearly, the nonrobustness of the fitted parameters does not cause undue spread in our prediction for the force-velocity relationship. The

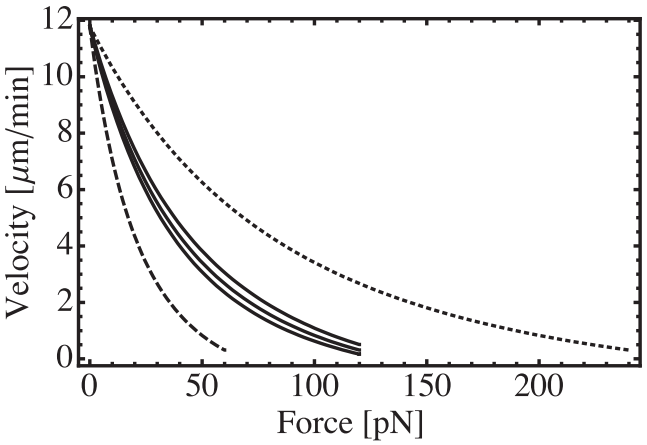

FIGURE 6 Force-velocity curve. (*Solid lines*) Results for the capping/nucleation rate ratio $\kappa/n = 0.05$ and three distinct sets of fitting parameters, all within the ranges shown in Table 3. (*Long-dashed line*) Results for $\kappa/n = 0.1$. (*Short-dashed line*) Results for $\kappa/n = 0.025$.

uncertainty in the value of the ratio κ/n does affect the results more severely, but the qualitative behavior remains the same.

Finally, we should point out the shortcomings of our model. In vivo, phosphorylation of MPOP in *A. suum* sperm cells is observed to be localized to discrete patches along the membrane (20). These regions of active MPOP are most likely responsible for the polymer dense regions (sometimes called ribs) that are observed in *A. suum* and *C. elegans* sperm cells (18,20,30). Modeling of *C. elegans* sperm motility suggests that these polymer dense regions may lead to larger crawling velocities than would be produced by a uniformly dense cytoskeleton (30). As little is known about what regulates this phosphorylation of MPOP, our model cannot describe the formation of these ribs, which may be important for describing protrusion in vivo. In addition, a complete catalog of the proteins involved in MSP polymerization is still lacking. Therefore, the model presented here is necessarily incomplete. However, since we were able to demonstrate that the putative roles of the known molecular players are consistent with the growth rate measurements, it is possible that these missing biochemical components are not present in limiting quantities.

We thank T. Roberts for a critical reading of the manuscript.

We acknowledge support from National Institutes of Health grants Nos. GM64346 and RR022232.

REFERENCES

1. Dao, D. N., R. H. Kessin, and H. L. Ennis. 2000. Developmental cheating and the evolutionary biology of *Dictyostelium* and *Myxococcus*. *Microbiology*. 146:1505–1512.
2. Rafelski, S. M., and J. A. Theriot. 2004. Crawling toward a unified model of cell motility: spatial and temporal regulation of actin dynamics. *Annu. Rev. Biochem*. 73:209–239.
3. Zigmond, S. H., and D. A. Lauffenburger. 1986. Assays of leukocyte chemotaxis. *Annu. Rev. Med.* 37:149–155.
4. Abercrombie, M. 1980. The Cronian lecture, 1978. The crawling movement of metazoan cells. *Proc. R. Soc. Lond. B. Biol. Sci*. 207:129–147.
5. Mitchison, T. J., and L. P. Cramer. 1996. Actin-based cell motility and cell locomotion. *Cell*. 84:371–379.
6. Lauffenburger, D. A., and A. F. Horwitz. 1996. Cell migration: a physically integrated molecular process. *Cell*. 84:359–369.
7. Grimm, H. P., A. B. Verkhovsky, A. Mogilner, and J. J. Meister. 2003. Analysis of actin dynamics at the leading edge of crawling cells: implications for the shape of keratocyte lamellipodia. *Eur. Biophys. J. Biophys. Lett*. 32:563–577.
8. Mullins, R. D., J. A. Heuser, and T. D. Pollard. 1998. The interaction of Arp2/3 complex with actin: nucleation, high-affinity pointed end capping, and formation of branching networks of filaments. *Proc. Natl. Acad. Sci. USA*. 95:6181–6186.
9. Pollard, T. D., L. Blanchoin, and R. D. Mullins. 2000. Molecular mechanisms controlling actin filament dynamics in nonmuscle cells. *Annu. Rev. Biophys. Biomol. Struct*. 29:545–576.
10. Machesky, L. M., and R. H. Insall. 1999. Signaling to actin dynamics. *J. Cell Biol*. 146:267–272.
11. Rohatgi, R., L. Ma, H. Miki, M. Lopez, T. Kirchhausen, et al. 1999. The interaction between N-WASP and the Arp2/3 complex links Cdc42-dependent signals to actin assembly. *Cell*. 97:221–231.
12. Winter, D., T. Lechler, and R. Li. 1999. Activation of the yeast Arp2/3 complex by Bee1p, a WASP-family protein. *Curr. Biol*. 9:501–504.
13. Yarar, D., W. To, A. Abo, and M. D. Welch. 1999. The Wiskott-Aldrich syndrome protein directs actin-based motility by stimulating actin nucleation with the Arp2/3 complex. *Curr. Biol*. 9:555–558.
14. Schafer, D. A., P. B. Jennings, and J. A. Cooper. 1996. Dynamics of capping protein and actin assembly in vitro: uncapping barbed ends by polyphosphoinositides. *J. Cell Biol*. 135:169–179.
15. DiNubile, M. J., L. Cassimeris, M. Joyce, and S. H. Zigmond. 1995. Actin filament barbed-end capping activity in neutrophil lysates: the role of capping protein $\beta 2$. *Mol. Biol. Cell*. 6:1659–1671.
16. Mullins, R. D., and T. D. Pollard. 1999. Rho-family GTPases require the Arp2/3 complex to stimulate actin polymerization in *Acanthamoeba* extracts. *Curr. Biol*. 9:405–415.
17. Mogilner, A. 2009. Mathematics of cell motility: have we got its number? *J. Math. Biol*. 58:105–134.
18. Sepsenwol, S., H. Ris, and T. M. Roberts. 1989. A unique cytoskeleton associated with crawling in the amoeboid sperm of the nematode, *Ascaris suum*. *J. Cell Biol*. 108:55–66.
19. Bullock, T. L., T. M. Roberts, and M. Stewart. 1996. 2.5 Å resolution crystal structure of the motile Major Sperm Protein (MSP) of *Ascaris suum*. *J. Mol. Biol*. 263:284–296.
20. LeClaire III, L. L., M. Stewart, and T. M. Roberts. 2003. A 48 kDa integral membrane phosphoprotein orchestrates the cytoskeletal dynamics that generate amoeboid cell motility in *Ascaris* sperm. *J. Cell Sci*. 116:2655–2663.
21. Buttery, S. M., G. C. Ekman, M. Seavy, M. Stewart, and T. M. Roberts. 2003. Dissection of the *Ascaris* sperm motility machinery identifies key proteins involved in major sperm protein-based amoeboid locomotion. *Mol. Biol. Cell*. 14:5082–5088.
22. Yi, K., S. M. Buttery, M. Stewart, and T. M. Roberts. 2003. A Ser/Thr kinase required for membrane-associated assembly of the major sperm protein motility apparatus in the amoeboid sperm of *Ascaris*. *Biophys. J*. 84:1591–1605.
23. Italiano, Jr., J. E., T. M. Roberts, M. Stewart, and C. A. Fontana. 1996. Reconstitution in vitro of the motile apparatus from the amoeboid sperm of *Ascaris* shows that filament assembly and bundling move membranes. *Cell*. Vol. 84:105–114.
24. Giardini, P. A., D. A. Fletcher, and J. A. Theriot. 2003. Compression forces generated by actin comet tails on lipid vesicles. *Proc. Natl. Acad. Sci. USA*. 100:6493–6498.

25. Grant, R. P., S. M. Buttery, G. C. Ekman, T. M. Roberts, and M. Stewart. 2005. Structure of MFP2 and its function in enhancing MSP polymerization in *Ascaris* sperm amoeboid motility. *J. Mol. Biol.* 347:583–595.

26. Bottino, D., A. Mogilner, T. Roberts, M. Stewart, and G. Oster. 2002. How nematode sperm crawl. *J. Cell Sci.* 115:367–384.

27. Mogilner, A., and D. W. Verzi. 2003. A simple 1-D physical model for the crawling nematode sperm cell. *J. Stat. Phys.* 110:1169–1189.

28. Wolgemuth, C. W., L. Miao, O. Vanderlinde, T. Roberts, and G. Oster. 2005. MSP dynamics drives nematode sperm locomotion. *Biophys. J.* 88:2462–2471.

29. Joanny, J. F., F. Jülicher, and J. Prost. 2003. Motion of an adhesive gel in a swelling gradient: a mechanism for cell locomotion. *Phys. Rev. Lett.* 90:168102.

30. Zajac, M., B. Dacanay, W. A. Mohler, and C. W. Wolgemuth. 2008. Depolymerization-driven flow in nematode spermatozoa relates crawling speed to size and shape. *Biophys. J.* 94:3810–3823.

31. Mogilner, A., and G. Oster. 2003. Force generation by actin polymerization II: the elastic ratchet and tethered filaments. *Biophys. J.* 84:1591–1605.

32. Bullock, T. L., A. J. McCoy, H. M. Kent, T. M. Roberts, and M. Stewart. 1998. Structural basis for amoeboid motility in nematode sperm. *Nat. Struct. Mol. Biol.* 5:184–189.

33. Peskin, C. S., G. M. Odell, and G. F. Oster. 1993. Cellular motions and thermal fluctuations: the Brownian ratchet. *Biophys. J.* 65:316–324.

34. Mogilner, A., and G. Oster. 1996. Cell motility driven by actin polymerization. *Biophys. J.* 71:3030–3045.

35. Miao, L., O. Vanderlinde, J. Liu, R. P. Grant, A. Wouterse, et al. 2008. The role of filament-packing dynamics in powering amoeboid cell motility. *Proc. Natl. Acad. Sci. USA.* 105:5390–5395.